

Monolayer Mirrors Under Strain: Manipulation of Optical Anisotropy in Borophene

Lyudmyla Adamska¹ and Sahar Sharifzadeh^{1,2,}*

¹ Department of Electrical and Computer Engineering, Boston University, Boston, Massachusetts 02215, United States

² Department of Physics and Division of Materials Science, Boston University, Boston, Massachusetts 02215, United States

CORRESPONDING AUTHOR FOOTNOTE: * ssharifz@bu.edu

DATE SUBMITTED: June 16, 2017

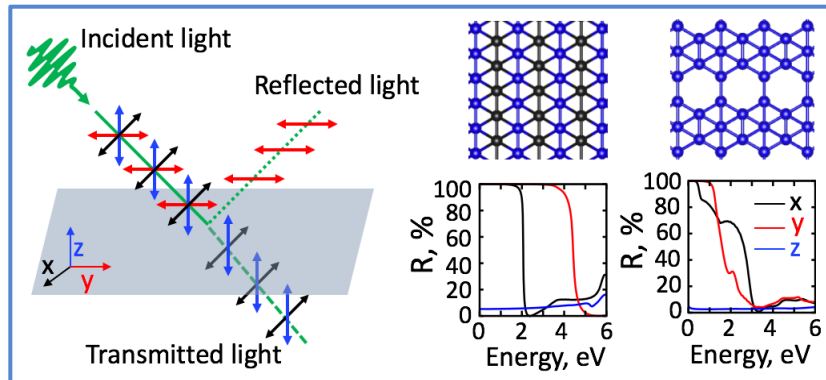
ABSTRACT

Two-dimensional boron (borophene) is a promising, newly synthesized monolayer metal with promising electronic and optical properties. Borophene has only been recently synthesized on silver substrates, and displays a variety of crystal structures and substrate-induced strains depending on growth conditions and surface orientation. Here, we present an extensive first-principles study of the structural and optoelectronic properties of the two proposed structures of borophene, β_{12} and δ_6 , under strain. With a density functional theory analysis, we determine that optical transparency and electronic band structure are continuously tunable upon application of few percent of strain. While both structures remain metallic with moderate strains of up to 6% applied, key features of the bandstructure, as well as in-plane anisotropy of optical transmittance

and reflectance can be significantly modified. In the visible range, these strained boron sheets are on average 50% transparent for in-plane polarized light and over 95% transparent for light polarized perpendicular to the surface, within an energy window that can be modified by strain, making borophene a promising monolayer mirror.

KEYWORDS: borophene, two-dimensional metal, optical reflectance, density functional theory

SYNOPSIS TOC



I. Introduction

Nanoscale conductors such as graphene and carbon nanotubes are the key functional elements in several next-generation nanotechnologies. In particular, ultrathin carbon-based films have been recently utilized in next-generation touchscreen technologies,^{1,2} flexible electronics,³ transparent conductive electrodes in solar cells,^{4–6} and low-power electronics.^{7,8} These materials have low production costs and scalable processing methods; however, in sub-10 nm devices, with atomically controlled interfaces, it is particularly desirable to have a defect-free atomically thin monolayer that can serve as an electrode. While exfoliated graphene is highly promising for this application, there are remaining challenges for large-scale production. CVD-grown graphene samples have micron-sized grains⁹ and reduced graphene oxide has residual defects^{10,11} which degrade the conductivity of the sheet. As an alternative, two-dimensional (2D) boron or borophene is a recently proposed monolayer material that has been predicted to display metallic properties,^{12–15} and form Ohmic contacts to 2D semiconductors, greatly enhancing the performance of electronic devices.¹⁶

Borophene has only been recently synthesized on silver substrates^{17–20} with STM images providing evidence of the 2D nature of the films, though the crystal structure is still undetermined due the many possible low-energy structures. Solid boron exists in numerous allotropes: there are four bulk boron structures,²¹ and as the dimensions are reduced to two,^{12,14,15,22–30} one^{14,31–35} or zero,^{36–40} multiple low-energy structures have been observed and predicted. To date, the true ground state structure of the monolayer is not known.^{22,25,27,41–44} It is predicted that planar boron sheets form a triangular bonding configuration which is unstable due to an excess of electrons that occupy anti-bonding orbitals;^{12,13} this structure can be stabilized by

the introduction of vacancies, an example of which is shown for the β_{12} structure in Figure 1a, or out-of-plane buckling as shown for the δ_6 structure in Figure 1b. Additionally, when borophene is grown on substrates, the lattice mismatch between the substrate lattice constant and the periodicity of the boron sheet, as well as charge transfer between boron and substrate, favor certain atomic configurations of boron atoms (boron allotropes) and rotation angles between boron and substrate (Moire patterns). There are several experimentally observed structures for borophene grown on Ag(111) based on scanning tunneling microscopy (STM) measurements and calculations. The δ_6 structure, a hexagonal lattice with out-of-plane-rumpling of the central atom, was initially proposed as being consistent with STM measurements.¹⁷ The β_{12} structure, with one out of six boron atoms replaced by a vacancy, is expected to be the most abundantly grown on Ag(111) substrate,^{18,20,45} while at a higher growth temperatures, there is evidence for the χ_3 structure,²⁰ which has one out of five atoms missing and also forms a network of connected vacancies. Another structure, labeled alpha-boron, (1 out of 9 boron atoms missing)¹³ was predicted to be the lowest energy structure in two dimensions, but has been experimentally observed as only a minor phase on Ag(111) substrates.²⁰ Additionally, recent studies of borophene synthesized on Ag(110) substrates have demonstrated several new allotropes of borophene in striped phase with varying widths of stripes.¹⁹

To date, freestanding borophene has not yet been isolated and the electronic properties of the monolayer have not yet been measured. However, numerous *ab initio* calculations of borophene allotropes predict 2D metals with a rich set of electronic properties. Density functional theory (DFT) simulations, in particular, have demonstrated the very different electronic bandstructures of the different borophene allotropes.^{12–14,22,44,46–50} While all 2D allotropes are metallic, the bandstructure near the Fermi energy can take either a quadratic form as a traditional metal (e.g.,

for δ_6 sheets), or display both quadratic and crossing linear bands, resulting in Dirac points (e.g., β_{12} and χ_3). The Dirac point is above the Fermi level in β_{12} sheet and below the Fermi level in χ_3 sheet.⁵⁰ Additionally, phonon-mediated superconductivity⁵¹⁻⁵⁶ and low thermal conductivity⁵⁷ have been predicted for certain allotropes. Such diverse electronic properties of borophene allotropes, as well as their light weight, metallicity, and mechanical stability, suggest that it is a promising material for future applications as monolayer conductors, high-capacity electrodes for electrochemical applications,⁵⁸⁻⁶³ and metal-free catalysts for hydrogen evolution reaction.^{64,65}

This variety of experimentally synthesized borophene allotropes realized by change of substrate, the substrate crystallographic orientation, and growth conditions results in a rich variety of 2D metals. Additionally, small strains, induced by the adjustment of borophene to the substrate, can be utilized to tune the properties of borophene. Strain engineering has been extensively investigated for other 2D material systems such as graphene and transition metal dichalcogenides. As an example, homogeneous strain in graphene enhances electron-phonon coupling⁶⁶ and non-uniform strain generates extremely high pseudomagnetic fields.^{67,68} In monolayer molybdenum disulfide, small compressive (tensile) strains enhance (decrease) fluorescence intensity,^{69,70} and 10% tensile strain induces a semiconductor-to-metal transition.⁶⁹ Similar to these materials, borophene's mechanical strength is outstanding and the monolayer is expected to withstand high strains without reduction of structural integrity.^{50,71-77} However, a systematic study of strain engineering in this system has not been performed previously.

Here, we utilize first-principle density functional theory (DFT) to understand the in-plane strain-dependence of electronic and optical properties of two possible boron allotropes shown in Figure 1. We demonstrate that strain engineering in borophene allows for a continuous tuning of

electronic and optical properties without structural disintegration. We predict that both borophene structures are resilient to compressive and tensile strains up to 6%, with deformation energies of less than 100 meV; and that their bandstructures can be significantly modified at these strains while retaining its metallic nature. Moreover, we show that both boron allotropes are weakly absorbing and strongly reflecting at very low energies (<1 eV) but are semi-transparent in the visible range and almost fully transparent in the UV range, with the onset of transparency highly sensitive to strain. This tunability of reflectivity and transparency is important for future technological applications of borophene as a monolayer mirror or transparent conductor. Our study demonstrates that strain enhances the functionality of this promising 2D conductor via tuning of electronic and optical properties.

II. Results

A. Structural Properties

We study strain within two crystal structures of borophene, β_{12} and δ_6 , as depicted in Figure 1. These structures have been predicted as candidates for borophene grown on Ag(111), based on the symmetry of scanning tunneling microscopy (STM) images. While the β_{12} structure has been theoretically predicted to be the most favorable geometry on noble metal substrates,⁷⁸ the δ_6 structure is close in energy²² and its 1x3 supercell displays a close lattice match to the Ag(111) 1x $\sqrt{3}$ supercell. Here, we predict that the formation energy of the β_{12} structure on Ag(111) is 0.155 eV more favorable than the δ_6 structure, in agreement with previous DFT-based predictions.⁷⁸

Figure 2 illustrates the change of total energy of borophene as a function of strain along the x and y axes, $\varepsilon_{x,y}$, with 1% strain increments. The application of strain results in an energy penalty due to deformation (deformation energy) that we separate in three regimes—weak, moderate, or strong—based on magnitude. We classify the deformation as weak if the energy penalty is below 50 meV/atom; moderate if the energy penalty is between 50 meV to 100 meV per boron atom; and strong with deformation energies greater than 100 meV/atom.

The β_{12} structure (Figure 1a) contains 5 atoms per unit cell with alternating rows of empty and filled hexagons along the x-direction (forming stripes of vacancies along x) and columns of continuous line of atoms alternating with incomplete hexagons along the y-direction. Evaluation of the computed charge density indicates that the boron atoms are sp-bonded with delocalized charge density along x and a slightly weaker delocalization along y due to the different bond lengths in each direction (see Supporting Information Figures S1 and S2). Because the sp-type bonding in this structure is highly sensitive to atomic orbital overlap, the density localizes upon bond stretching (for tensile strain), and results in a less free-electron-like system. Similarly, compressive strains result in stronger density delocalization. The deformation energies upon application of strain, shown in Figure 2a, do not reflect this weak anisotropy; the deformation energy has relatively uniform behavior along the x and y directions. Here, small (1-2%) tensile or compressive strain results in a small energy penalty of about $k_B T$ (25 meV/atom); therefore, this material may easily slightly adjust its lattice constant to that of the underlying substrate. This weak deformation lasts up to strains of $(\varepsilon_x, \varepsilon_y) = (\pm 3, \pm 3)\%$, with an energy penalty of about 50 meV/atom. Uniaxial strains of $(\pm 6, 0)\%$ and $(0, \pm 6)\%$ result in moderate deformations of about 100 meV/atom, while biaxial (6,6)% tensile and (-6,-6)% compressive strains result in greater

than 150 meV/atom energy penalty, indicating a strong deformation. Beyond this region, the deformation energies are greater than 150 meV/atom.

By contrast, the δ_6 structure, shown in Figure 1b, contains 2 atoms in the hexagonal unit cell, with an out-of-plane rumpling of the central atom and no vacancy or stripe formation. Along the x-direction, the structure contains zigzagged rows with boron atoms of alternating heights, while along y, there are continuous columns of atoms. Here, analysis of the computed charge density suggests that the atoms bond via π -bonding of p_z orbitals. Due to the zigzag structure along x, the p_z orbital bonding is significantly weaker along this than along y as can be seen in the charge density distribution (see Figure S3 in Supporting Information). This anisotropy is reflected in deformation energies shown in Figure 2b: the δ_6 allotrope is soft towards deformations along the x-axis, as is expected based on the periodically buckled atomic configuration, and more difficult to deform along y. For example, with 10% strain, the deformation energy is ~100 meV/atom for both tensile and compressive strains along x, and 200 meV/atom and 500 meV/atom for tensile and compressive strains along y, respectively. Such large differences in compression energies are to be expected because compression along y-axis changes the bond lengths significantly. We predict that $\pm 3\%$ strain results in weak deformation and $\pm 6\%$ strain along the x-axis and y-axis, results in moderate and strong deformations, respectively.

Figure 2 indicates that $\pm 3\%$ (weak) and $\pm 6\%$ (moderate) strain, with few exceptions, do not result in a large deformation energy and thus will not compromise the structural integrity of the boron monolayers. Therefore, we focus on strains up to $\pm 6\%$ for further analysis. White circles in Figure 2 mark the values of strain, in 3% increments, for which we simulate the electronic and optical properties.

B. Optoelectronic Properties of Unstrained Borophene

In a separate study, we have carefully analyzed the optoelectronic properties of unstrained and the accuracy of DFT within the local density approximation (LDA) for describing these properties. We found, by comparison to many-body perturbation theory calculations, that DFT-LDA and RPA can accurately describe the bandstructure and optical absorption properties of borophene, respectively.⁷⁹ Our current study, which employs the PBE functional in order to better describe the structural properties of borophene, agrees well with these previous studies, as we briefly describe here. Figure 3 shows the calculated bandstructure for both unstrained structures. We predict that both allotropes are metals with several bands crossing the Fermi energy (E_F), in agreement with previous calculations.^{17,18,50,51,80,81} The β_{12} allotrope contains three bands near the top of the valence band (Figure 3a) and a Dirac cone, i.e., linearly crossing bands, located near the S-point at about 0.5 eV above E_F .⁸¹ The δ_6 structure shows a different character to the bandstructure, with two partially occupied bands which cross E_F , as shown in Figure 3b. In the vicinity of the Γ -point ($k = \mathbf{0}$), there is a ~4 eV gap in the bandstructure. Our calculations for the bandstructure of both borophene allotropes are in agreement published works that used similar DFT methodology.^{17,18,50,51,80,81} However, there is discrepancy between our calculations and those presented by Peng *et al.* (Ref.⁴⁹), which is likely due to the use of different DFT functionals (HSE06⁸² versus PBE⁸³).

The optical properties of two boron allotropes are presented in the lower panels of Figure 3. Here, we consider only inter-band transitions for optical absorption and ignore intra-band transitions that would result in modification of the spectrum at very low energies (< 0.1 eV). Both allotropes are predicted to be weakly absorbing: in the visible range, the absorbance is

under 1%. For comparison, within the same region of light, graphene absorbs 2.3%.⁸⁴ The onset of absorption is negligible (< 0.2 eV) for the β_{12} (Fig. 3a) structure and 3.5 eV for δ_6 (Fig. 3b) structure, consistent with the lowest direct transition energies in the bandstructure. We note Peng *et al.*⁴⁹ predict a different absorption spectrum, which can again be attributed to use of different functionals.

Interestingly, in contrast to graphene, which is fully transmitting in the visible region (transmits 96% of light⁸⁵), the borophene allotropes are strongly reflecting at low energy.⁷⁹ The β_{12} allotrope reflects light at low energies, starts to weakly transmit X- and Y-polarized light at energies larger than 1 eV, in the near-IR and visible ranges, and is strongly transmitting (>80%) in the violet and UV regions. The δ_6 allotrope is almost fully reflecting at low energies and is >90% transparent for light > 2 eV with X-polarized light, while for Y-polarized light, there is no transmission until the UV region with energies greater than 3.9 eV, after which the transmission is >90%. As is expected for a free-electron system, the energy of the reflectivity drop is determined by the plasma frequencies (ω_p) which are predicted to be 2.9 eV (2.4 eV) and 2.1 eV (4.4 eV) for X- (Y-) polarized light within the β_{12} and δ_6 allotropes, respectively. Both allotropes are >96% transparent for Z-polarized light.

Both borophene allotropes are partially transparent, but neither structure would be suitable as a transparent conductor in lieu of graphene due to the lack of transparency at low energies. However, borophene can serve as a polarization filter in the δ_6 structure: between 2 eV (orange light) and 3.9 eV (ultraviolet), the monolayer is a perfect polarization filter: it transmits 99% of X-polarized light and reflects 100% of Y-polarized light. Additionally, the 99% reflectance of X-

and Y-polarized light for either allotrope in the microwave region would suggest borophene as a promising as a monolayer mirror for this region of light.

C. Band structure of Strained Borophene

1. Strained β_{12} borophene

Figure 4 plots the band structure of strained β_{12} borophene, shown for $\pm 6\%$ strain in order to highlight the most important trends, which are observed to a lesser degree with $\pm 3\%$ strain. The most relevant features are highlighted in red circles (the Dirac point near S) and green ovals (the valence bands in vicinity of the Γ -point). In general, strain along the x-axis does not significantly alter the former but does strongly influence the latter, while strains along the y-axis strongly influence both.

Strain along y results in shifting of the Dirac point closer to E_F for compressive and farther away from E_F for tensile strains. This trend is most apparent when starting from an x-strained structure (panel (6, 0)) and straining along y. Upon stretching by 6% along y (panel (6, 6)), the Dirac point decreases to 0.1 eV above E_F , while 6% compression along y (panel (6, -6)) results in the Dirac point increasing to 0.9 eV above E_F . This suggests that tensile strength can lead to the presence of massless fermions at E_F as exist in graphene, though in this case there are parabolic bands resulting in massive electrons, present at E_F as well.

The gap near Γ is influenced by both x- and y-strain, with a greater influence of x-strain. The gap can open up from 0.1 eV with no strain to 0.8 eV with 6% tensile strain along x. As discussed in the next section, the value of this gap influences the nature and energy of the optical absorption onset. Additionally, the influence of strain along x- and y- axes are to some extent coupled as

both strain directions affect the highlighted electronic bands to some degree. 6% homogeneous tensile strain shifts the Dirac point to 0.1 eV above E_F and opens a 1 eV bandgap at Γ , while 6% compressive strain shifts the Dirac point to about 0.3 eV above E_F and results in closing of the bandgap in the vicinity of E_F near Γ .

2. Strained δ_6 borophene

For the strained δ_6 borophene, the two most relevant features are highlighted in Figure 5 by the blue arrow (gap at Γ) and red circle (unoccupied bands above the Fermi energy along Y- Γ line). As discussed in the next Section, these bands contribute to optical absorption in the visible range. In general, the bandgap at Γ is increased with compressive and decreased with tensile strains. Due to the anisotropic nature of the structure, there is anisotropy in this effect. Notably, a few percent deformation along the x-axis induces changes the gap by up to 2 eV for 6% strain ($(\pm 6, 0)$), while strain along y does not appreciably modify the gap (by ~ 0.5 eV in $(0, \pm 6)$). Because this structure shows small deformation energies along x, the strong response to strain in this direction may be unexpected, but can be explained based on its π -bonded nature and zigzag structure along x. The p_z orbitals are either pushed more out-of-plane with those of the neighboring atoms as borophene becomes more buckled under compression or pushed in-plane upon tensile x-directed strain resulting in stronger interactions among nearest-neighbors.

The unoccupied bands along the Y- Γ line are strongly responsive to strain along both x and y directions. The shape of the bands, as well as their position with respect to E_F , change with strain. For example, a 6% isotropic stretch ((6,6) panel) moves these bands by ~ 1.5 eV down towards E_F , while a 6% isotropic compression ((-6,-6) panel) pushes these bands up by ~ 2 eV

away from E_F . As these bands are lowered in energy below the gap at Γ , they begin to dominate optical absorption at low energies.

This analysis of the bandstructure indicates that both borophene allotropes remain metallic under weak and moderate strains. The strain-related changes to band shape, as well as their position with respect to the Fermi energy, will affect the conductivity of the monolayer metal, and will also affect energies and intensities of optical transitions as described in the next Section II.D.

D. Optical properties of Strained Borophene

With the application of strain, the weak absorbance, high reflectivity at low energies, and anisotropy of response to X/Y- light polarization described in Section II.B are maintained. However, there are two features that can be manipulated by strain i) the anisotropy between X and Y response, which is related to its application as a polarization filter; and ii) the onset of reflectivity decline/transmission rise which is related to its application as a monolayer mirror. As explained below, these strain-dependent trends can be related to the change in bandstructure and charge density delocalization.

1. Strained β_{12} borophene

Figure 6a shows the strain-dependent trends of optical absorbance in the β_{12} allotrope. The application of a few percent strain does not result in significant shift of the onset of absorption (which is close to zero) or in increase of absorption strength (< 1% absorptivity in the UV-visible region). Hence, for this system, transmission is essentially inversely related to reflectivity (neglecting absorption, $T = 1 - R$). As the material goes from highly reflective to non-reflective, the transmission increases (Figures 6b and 6c). All strained structures are highly reflecting at low

energies and drop in reflectivity at the plasma frequency (ω_p), which depends on the polarization of light. The strain-dependent ω_p are shown in the Supporting Information Table S3. For X-polarized light the ω_p ranges from 2.15 eV to 3.71 eV, while for Y-polarized light, it can vary from 0.64 eV to 3.44 eV. This indicates the energy of drop in reflectivity (i.e. the onset of transmission) can be modified to span the IR, visible, and near UV regions.

The shift in ω_p with strain also correlates with the strong enhancement or suppression of reflectivity. As an example, Table S5 shows the strength of reflectivity for light energy of 2.5 eV, chosen to be somewhere in the middle of the UV-visible region. For X-polarized light, the reflectivity of the unstrained structure is 70%, and this number can shift between 10-90% depending on the level of strain and follows trends in change of ω_p . Similarly for Y-polarized light, we predict a reflectivity of 15% for the unstained structure that can be shifted to 10-70% with strain and follows the trend of ω_p . Interestingly, going from the unstrained structure to one with applied strain along x- or y-, the density delocalization follows the trends in Table S3 (see calculated strain-dependent local density of states in Figures S1 and S2 in the Supporting Information).

Strain influences the X- and Y- response of β_{12} differently, allowing the anisotropy in response to be tuned. We show in Table S6 a measure of anisotropy as the difference between ω_p for X- and Y-polarization, which corresponds to drop of reflectance for respective polarizations of light, therefore quantifying the energy range where X- or Y- polarizations dominate. This value is 1 eV for the unstrained structure, indicating that X-polarized light begins to transmit at energy of 1 eV below Y-polarized light. The application of tensile strain along x increases the anisotropy, while compressive strain decreases it (see Table S7 for trends). Conversely, the application of tensile

strain along y decreases anisotropy, while compressive strain decreases it. Homogenous strain, either compressive or tensile, decreases anisotropy. These trends can be clearly understood as due to change in anisotropy of the atomic structure; for example, with homogeneous tensile strain, the bond-lengths shift such that the bond-length connecting the hexagonal rows is closer to the length of the hexagon edges, resulting in a more isotropic charge density (see calculated local density of states in Figures S1 and S2 in the Supporting Information).

2. Properties of strained δ_6 borophene

Figure 7a presents the variation of absorbance in δ_6 borophene as a function of strain. The application of strain results in dramatic shifts of the onset of absorption; this is to be expected based on the changes in the gap at Γ and the position of the lowest energy fully unoccupied band in the bandstructure as shown in Figure 4. We predict that compressive strains along x, y, or xy (homogeneous strain) increase while tensile strains in the same directions decrease the onset of absorption. Unstrained borophene (0,0) has onsets of absorption at 3.5 and 6.5 eV for X and Y polarized light, respectively. The most dramatic shift in onset is seen with the application of homogeneous strain 6% strain; tensile strain (panel (6,6)) reduces the onsets of absorption to 2 and 5 eV, while compression (panel (-6,-6)) increases the onsets to 4 and 8 eV for X and Y light polarizations, respectively.

For the δ_6 structure, there is no appreciable change in reflectivity strength within the UV-visible region with strain. As shown in Figure 7b, reflectivity is near 100% at low energies and falls abruptly to ~0% at ω_p , while transmission rises abruptly from 0% to ~100% at ω_p for all strains. As with the β_{12} , onsets as determined by ω_p can vary by a few eVs with applied strain (0.85-3.44 eV for X-polarized light and 0.64 to 3.44 eV for Y-polarized light) and strains significantly alter

the X-/Y- anisotropy, as shown in Table S4. The trend in strain-dependent X-/Y- anisotropy, shown in Tables S6 and S7, are not as clear for this structure because of the larger deformation at high (6%) strain and because of the non-planar structure. In general, compressive (tensile) strains along y increase (decrease) anisotropy, which can be explained as due to the decreased (increased) bond-lengths and therefore, increased (decreased) delocalization along y. For strains along x, there is a competition between change in buckling, which leads to increased delocalization as the buckling is reduced and the sheet becomes more planar (for tensile strain), and change in bond-lengths which separates p_z orbitals and reduces delocalization. As shown in Table S6, the anisotropy can be minimized with a strain of (-6,3) to 0.5 eV difference or maximized at a strain of (-3,-6) to 4.4 eV.

Such tunability of reflectance and transmittance thresholds makes δ_6 borophene a promising material for optical applications in which the optical transparency to visible light needs to be turned off and varies with polarization of light. Our studies suggest that the δ_6 allotrope can be a promising polarization filter, transmitting all X-polarized light and reflecting all Y-polarized light. Strain may remove the optical anisotropy in the β_{12} structure to create a polarization-independent mirror, which was not achievable for δ_6 borophene for the studied values of strain.

III. Conclusions

In summary, we have investigated the electronic and optical properties of two proposed allotropes of monolayer boron (borophene) upon application of tensile and compressive strains in order to simulate the influence of its underlying substrate and assess the tunability of its optoelectronic properties. We predict that the application of few percent strain changes the total energy by < 0.1 eV/atom thus not compromising its structural integrity. Our DFT-based

calculations reveal that the optical properties of borophene strongly respond to small strains, a feature that is correlated with enhancement or decrease of charge delocalization along different crystallographic directions by modification of bond lengths. Additionally, we demonstrate that the two structures respond in distinct ways to strain. For the β_{12} structure, there is an anisotropy of reflectance and transmittance for X- and Y-polarized light, which can be enhanced or fully eliminated via strain. For the δ_6 structure, applied strain also alters the onsets of reflectance and transmittance for X- and Y-polarized light and thus increases the energy window for light polarization filtering. This study demonstrates that strain can be utilized to tune the optoelectronic properties of borophene, increasing the applicability of borophene in 2D device architectures.

Computational Details

Density functional theory (DFT) and Random Phase Approximation (RPA) calculations on the strained β_{12} and δ_6 borophene structures were performed using the Quantum Espresso simulation suite.⁸⁶ We utilized the PBE functional⁸³ and Troullier-Martins⁸⁷ norm-conserving pseudopotentials to describe the core and nuclei of boron. In order to account for the aperiodicity of the isolated monolayer, we include 12 Å of vacuum between periodic images along direction perpendicular to the borophene. Convergence of the total energy was found to be better than 1 meV/atom for a plane wave cutoff 100 Ry and k-point mesh of 36×20x1 and 36×60x1 for the β_{12} and δ_6 structures, respectively, which corresponds to a k-point density of $2\pi\times0.01 \text{ \AA}^{-1}$.

The structure of the β_{12} and δ_6 unit cells were optimized within the xy plane to the accuracy of 0.01 meV/atom energy and 1 meV/Å force tolerance. The optimized unit cells were determined to be $(a_0, b_0) = (2.936 \text{ \AA}, 5.087 \text{ \AA})$, where a and b are the lattice vectors in x and y directions,

respectively for the β_{12} structure and $(a_0, b_0) = (2.892 \text{ \AA}, 1.615 \text{ \AA})$ for the δ_6 structure. Strained unit cells were constructed with 1% strain increment, with atomic positions re-optimized. Compressive and tensile strains were applied in the x and y directions. We label strain in x and y direction using such notations: $(\varepsilon_x, \varepsilon_y) = (\frac{a-a_0}{a_0}, \frac{b-b_0}{b_0}) \times 100\%$, with a negative strain indicating compression. The deformation energy was computed with $\pm 1\%$ strain increments as $E_{def}(\varepsilon_x, \varepsilon_y) = E_{tot}(\varepsilon_x, \varepsilon_y) - E_{tot}(0,0)$. Figure 2 shows a heat map of deformation energies for 440 values of strain for each boron allotrope.

The detailed analysis of the electronic structure of strained borophene was performed for ± 3 and ± 6 percent of strain. For bandstructure calculations, the coordinate of high symmetry points in (k_x, k_y) space were the following: $\Gamma=(0.0, 0.0)$, $X=(\pi/a, 0.0)$, $Y=(0.0, \pi/b)$, $S=(\pi/a, \pi/b)$. The density of k-points along chosen high-symmetry directions was set to $2\pi \times 0.005 \text{ \AA}^{-1}$. Band structure plots, depicted in Figures 4 and 5, were shifted by the E_F energy, calculated on a homogeneous k-grid. The work function for each strained geometry is shown in Table S2.

We employ the RPA to calculate complex dielectric function $\epsilon_1 + i\epsilon_2$ of strained boron allotropes. Intraband transitions were neglected in this work. We compute the optical absorbance as $A = \frac{\omega}{c} L \epsilon_2$, reflectance as $R = \frac{(1-n)^2+k^2}{(1+n)^2+k^2}$, and transmittance, $T = 1 - R - A$, for 25 strained geometries ranging from -6% to 6% strain. Here, n and k are the real and imaginary components of the refractive index which are related to the real and imaginary component of the dielectric function as $\epsilon_1 = n^2 - k^2$ and $\epsilon_2 = 2nk$; and L is the thickness of the simulation cell in the z direction, i.e. perpendicular to borophene. In order to simulate the broadening of the dielectric function due to finite temperature, we used a Gaussian smearing of width 0.2 eV. For the 25

strained structures, the k-point mesh was kept at 36x20x1 and 36x60x1 for the β_{12} and δ_6 boron allotropes, respectively. While this k-point mesh is sufficient for capturing strain-dependents trends in optoelectronic properties, a higher density k-point mesh of 180x100x1 and 180x300x1 for β_{12} and δ_6 systems, respectively, was required to eliminate noise. Due to the high computational cost, we only used this dense k-point mesh to study the unstrained structures, with the results shown in Figure 3.

In order to better understand the enhanced anisotropy of reflectance and transmittance in selected strained geometries, we calculated the local density of states (LDOS) near the Fermi energy by summing the square of the wave functions for all states with eigenvalues between energies (E_F , $E_F + 100$ meV) and ($E_F - 100$ meV, E_F) for all k-points. The results are plotted in Figure S1 and S3. The slices of LDOS at 0.8 Å above the atomic plane are shown in Figure S2.

ACKNOWLEDGMENTS

The authors acknowledge the computational resources through Center for Nanomaterials at Argonne National Laboratory, an Office of Science user facility, supported by the U. S. Department of Energy, Office of Science, Office of Basic Energy Sciences, under Contract No. DE-AC02-06CH11357; and the Extreme Science and Engineering Discovery Environment (XSEDE), which is supported by National Science Foundation grant number ACI-1548562. The authors acknowledge financial support from Boston University and L.A. acknowledges support through BUnano postdoctoral fellowship. The authors are grateful for fruitful discussions with Dr. Pierre Darancet of Argonne National Laboratory.

SUPPORTING INFORMATION

Supporting information document contains figures related to the spatial analysis of the electron density in the vicinity of the Fermi level, and tables with data related to electronic properties of strained borophene.

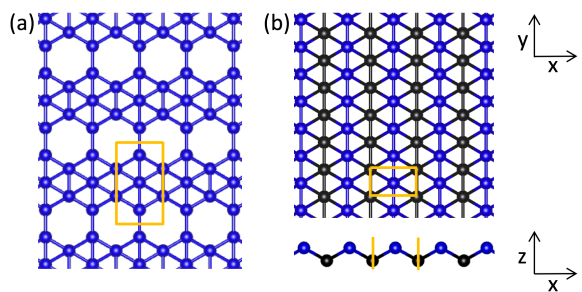


Figure 1. Atomic structure of the (a) β_{12} and (b) δ_6 borophene phases. The unit cell for each is shown by an orange box. The β_{12} and δ_6 phases have 5 and 2 boron atoms per unit cell, respectively with the δ_6 phase displaying an out-of-plane rippling of 0.88 Å as shown at the bottom of (b). The definition of x, y, and z directions are labeled. <-- need to also label beta_12.

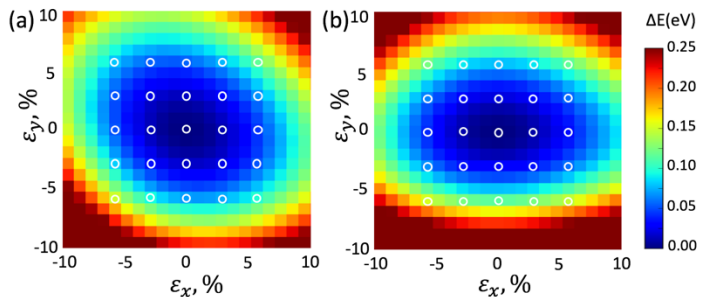


Figure 2. Deformation energy per atom (eV) as a function of strain $\varepsilon_{x,y}$ in the (a) β_{12} and (b) δ_6 borophene. One pixel corresponds to 1% increments in value of strain. White circles mark the values of strain $\varepsilon_{x,y} = (0, \pm 3, \pm 6)\%$ that were studied in more details.

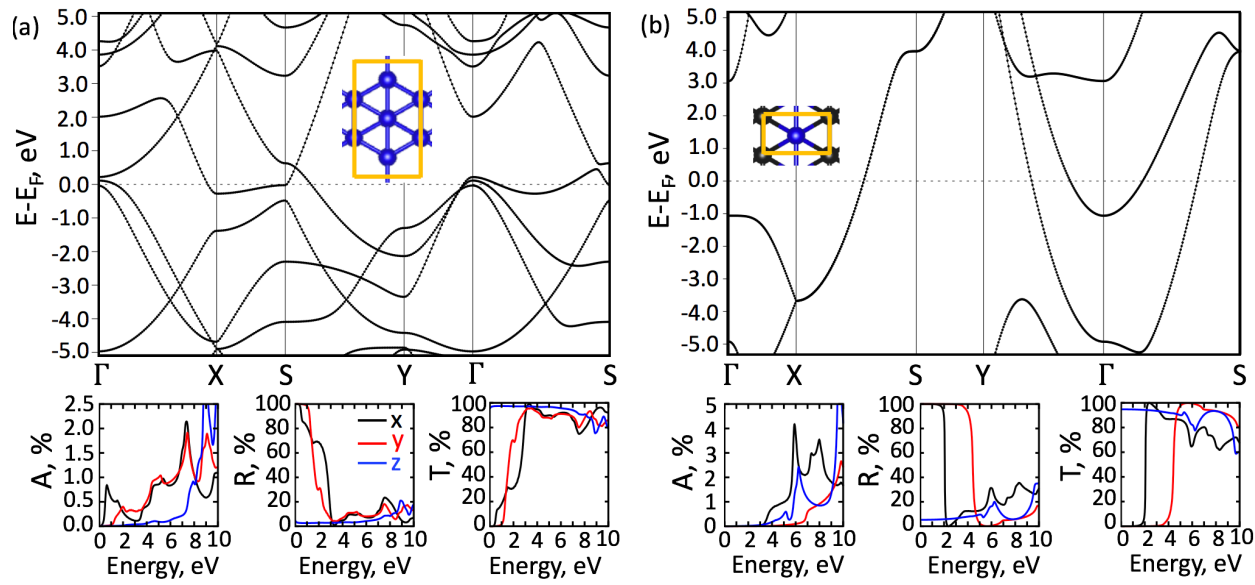


Figure 3. Band structure of unstrained β_{12} (left) and δ_6 (right) borophene cells. Absorbance (A), reflectance (R), and transmittance (T) and shown for each geometry. X, Y, and Z polarizations of light are depicted in black, red, and blue colors, respectively. The coordinates of high symmetry points in (k_x, k_y) space are the following: $\Gamma=(0.0, 0.0)$, $X=(\pi/a, 0.0)$, $Y=(0.0, \pi/b)$, $S=(\pi/a, \pi/b)$. The plots are shifted such that the Fermi energy (dotted line) is at zero.

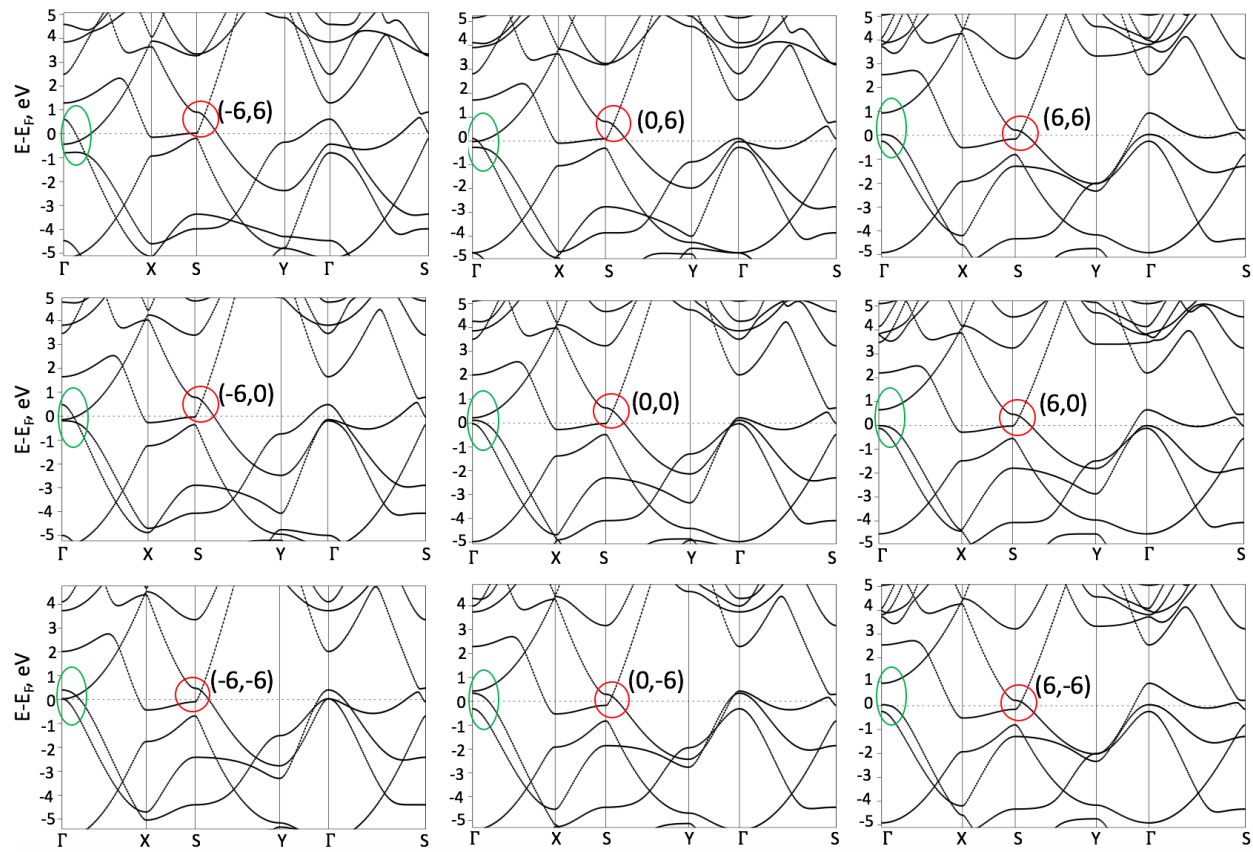


Figure 4. Band structure of β_{12} borophene at selected values of strain. Red circles highlight the changes in the position of the Dirac point and green ovals accentuate the alteration of band structure in the vicinity of the Γ -point. The assignment of high symmetry points in the band structure is shown in caption to Figure 3.

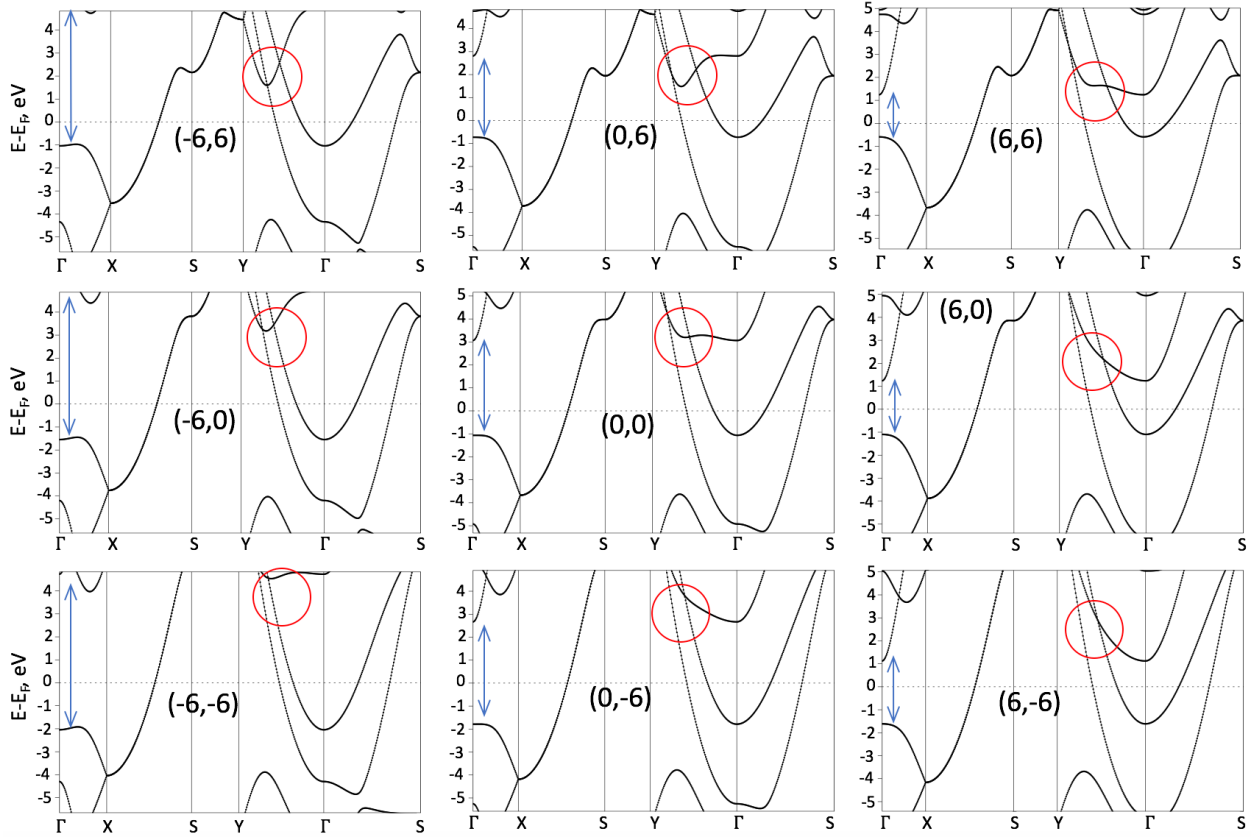


Figure 5. Band structure of δ_6 borophene at selected values of strain. Red circles and blue arrows highlight the important changes in the band structure along Γ -Y and at the Γ -point, respectively. The assignment of high symmetry points in the band structure is shown in caption to Figure 3.

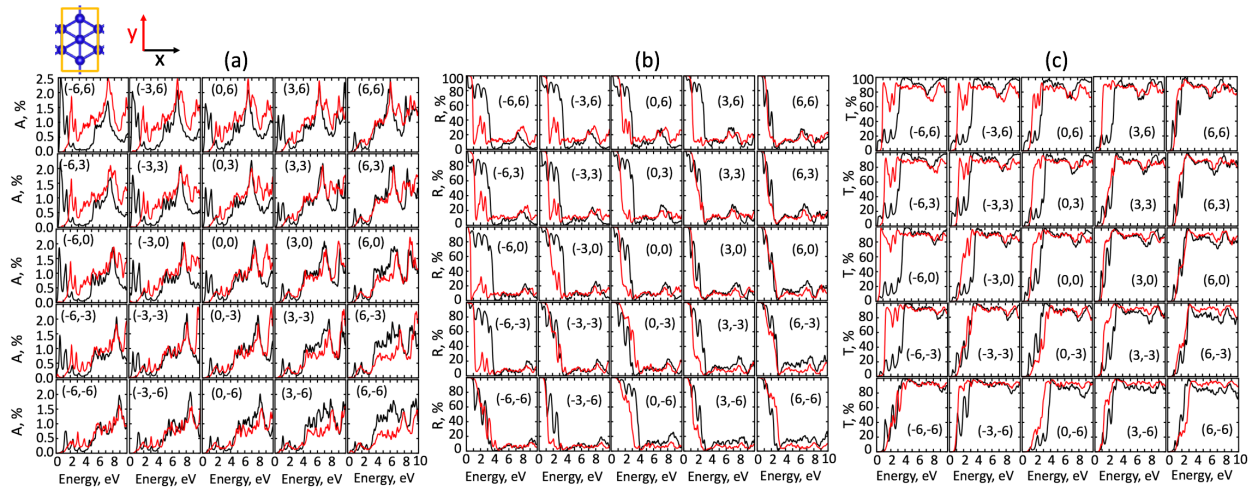


Figure 6. (a) Optical absorbance, (b) reflectance and (c) transmittance in strained β_{12} borophene as a function of energy of incident light. X and Y polarization of light are depicted in black and red colors, respectively.

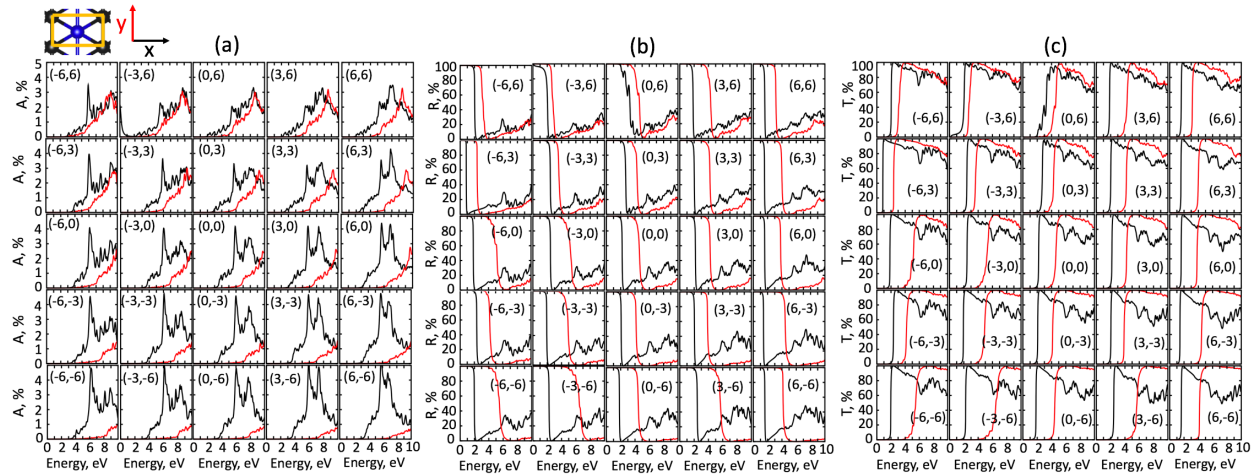


Figure 7. (a) Optical absorbance, (b) reflectance and (c) transmittance in strained δ_6 borophene as a function of energy of incident light. X and Y polarization of light are depicted in black and red colors, respectively.

REFERENCES

- (1) Li, Z.; Liu, Z.; Sun, H.; Gao, C. Superstructured Assembly of Nanocarbons: Fullerenes, Nanotubes, and Graphene. *Chem. Rev.* **2015**, *115* (15), 7046–7117.
- (2) Schindler, A.; Brill, J.; Fruehauf, N.; Novak, J. P.; Yaniv, Z. Solution-Deposited Carbon Nanotube Layers for Flexible Display Applications. *Phys. E Low-dimensional Syst. Nanostructures* **2007**, *37* (1–2), 119–123.
- (3) Liu, Y.; Zhou, H.; Cheng, R.; Yu, W.; Huang, Y.; Duan, X. Highly Flexible Electronics from Scalable Vertical Thin Film Transistors. *Nano Lett.* **2014**, *14* (3), 1413–1418.
- (4) Wang, X.; Zhi, L.; Mu, K. Transparent , Conductive Graphene Electrodes for Dye-Sensitized Solar Cells. **2008**.
- (5) Tenent, R. C.; Barnes, T. M.; Bergeson, J. D.; Ferguson, A. J.; To, B.; Gedvilas, L. M.; Heben, M. J.; Blackburn, J. L. Ultrasmooth, Large-Area, High-Uniformity, Conductive Transparent Single-Walled-Carbon-Nanotube Films for Photovoltaics Produced by Ultrasonic Spraying. *Adv. Mater.* **2009**, *21* (31), 3210–3216.
- (6) Kim, S.; Yim, J.; Wang, X.; Bradley, D. D. C.; Lee, S.; deMello, J. C. Spin- and Spray-Deposited Single-Walled Carbon-Nanotube Electrodes for Organic Solar Cells. *Adv. Funct. Mater.* **2010**, *20* (14), 2310–2316.
- (7) Heo, J.; Byun, K.-E.; Lee, J.; Chung, H.-J.; Jeon, S.; Park, S.; Hwang, S. Graphene and Thin-Film Semiconductor Heterojunction Transistors Integrated on Wafer Scale for Low-Power Electronics. *Nano Lett.* **2013**, *13* (12), 5967–5971.

- (8) Hlaing, H.; Kim, C.-H.; Carta, F.; Nam, C.-Y.; Barton, R. A.; Petrone, N.; Hone, J.; Kymissis, I. Low-Voltage Organic Electronics Based on a Gate-Tunable Injection Barrier in Vertical Graphene-Organic Semiconductor Heterostructures. *Nano Lett.* **2015**, *15* (1), 69–74.
- (9) Huang, P. Y.; Ruiz-Vargas, C. S.; van der Zande, A. M.; Whitney, W. S.; Levendorf, M. P.; Kevek, J. W.; Garg, S.; Alden, J. S.; Hustedt, C. J.; Zhu, Y.; et al. Grains and Grain Boundaries in Single-Layer Graphene Atomic Patchwork Quilts. *Nature* **2011**, *469* (7330), 389–392.
- (10) Stankovich, S.; Dikin, D. A.; Piner, R. D.; Kohlhaas, K. A.; Kleinhammes, A.; Jia, Y.; Wu, Y.; Nguyen, S. T.; Ruoff, R. S. Synthesis of Graphene-Based Nanosheets via Chemical Reduction of Exfoliated Graphite Oxide. *Carbon N. Y.* **2007**, *45* (7), 1558–1565.
- (11) Yamaguchi, H.; Ogawa, S.; Watanabe, D.; Hozumi, H.; Gao, Y.; Eda, G.; Mattevi, C.; Fujita, T.; Yoshigoe, A.; Ishizuka, S.; et al. Valence-Band Electronic Structure Evolution of Graphene Oxide upon Thermal Annealing for Optoelectronics. *Phys. status solidi* **2016**, *213* (9), 2380–2386.
- (12) Tang, H.; Ismail-Beigi, S. Self-Doping in Boron Sheets from First Principles: A Route to Structural Design of Metal Boride Nanostructures. *Phys. Rev. B - Condens. Matter Mater. Phys.* **2009**, *80* (13), 1–8.
- (13) Tang, H.; Ismail-Beigi, S. Novel Precursors for Boron Nanotubes: The Competition of Two-Center and Three-Center Bonding in Boron Sheets. *Phys. Rev. Lett.* **2007**, *99* (11), 12–15.

- (14) Tang, H.; Ismail-Beigi, S. First-Principles Study of Boron Sheets and Nanotubes. *Phys. Rev. B - Condens. Matter Mater. Phys.* **2010**, *82* (11), 1–20.
- (15) Evans, M. H.; Joannopoulos, J. D.; Pantelides, S. T. Electronic and Mechanical Properties of Planar and Tubular Boron Structures. *Phys. Rev. B - Condens. Matter Mater. Phys.* **2005**, *72* (4), 1–6.
- (16) Liu, L. Z.; Xiong, S. J.; Wu, X. L. Monolayer Borophene Electrode for Effective Elimination of Both the Schottky Barrier and Strong Electric Field Effect. *Appl. Phys. Lett.* **2016**, *109* (6), 61601.
- (17) Mannix, A. J.; Zhou, X.; Kiraly, B.; Wood, J. D.; Alducin, D.; Myers, B. D.; Liu, X.; Fisher, B. L.; Santiago, U.; Guest, J. R.; et al. Synthesis of Borophenes: Anisotropic, Two-Dimensional Boron Polymorphs. **2015**, *350* (6267), 1513–1516.
- (18) Feng, B.; Zhang, J.; Zhong, Q.; Li, W.; Li, S.; Li, H.; Cheng, P.; Meng, S.; Chen, L.; Wu, K. Experimental Realization of Two-Dimensional Boron Sheets. *Nat Chem* **2016**, *8* (6), 563–568.
- (19) Zhong, Q.; Kong, L.; Gou, J.; Li, W.; Sheng, S.; Yang, S.; Cheng, P.; Li, H.; Wu, K.; Chen, L. Synthesis of Borophene Nanoribbons on Ag(110) Surface. **2017**, No. 110.
- (20) Zhong, Q.; Zhang, J.; Cheng, P.; Feng, B.; Li, W.; Sheng, S.; Li, H.; Meng, S.; Chen, L.; Wu, K. Metastable Phases of 2D Boron Sheets on Ag(1 1 1). *J. Phys. Condens. Matter* **2017**, *29* (9), 95002.
- (21) Parakhonskiy, G.; Dubrovinskaia, N.; Bykova, E.; Wirth, R.; Dubrovinsky, L.

Experimental Pressure-Temperature Phase Diagram of Boron: Resolving the Long-Standing Enigma. *Sci. Rep.* **2011**, *1*, 96.

- (22) Wu, X.; Dai, J.; Zhao, Y.; Zhuo, Z.; Yang, J.; Zeng, X. C. Two-Dimensional Boron Monolayer Sheets. *ACS Nano* **2012**, *6* (8), 7443–7453.
- (23) Karmodak, N.; Jemmis, E. D. The Role of Holes in Borophenes: An Ab Initio Study of Their Structure and Stability with and without Metal Templates. *Angew. Chem. Int. Ed. Engl.* **2017**, 1–6.
- (24) Tarkowski, T.; Majewski, J. A.; Szwacki, N. G. Energy Decomposition Analysis of Neutral and Negatively Charged Borophenes. **2016**, 1–4.
- (25) Liu, Y.; Penev, E. S.; Yakobson, B. I. Probing the Synthesis of Two-Dimensional Boron by First-Principles Computations. *Angew. Chemie - Int. Ed.* **2013**, *52* (11), 3156–3159.
- (26) Zhang, Z.; Penev, E. S.; Yakobson, B. I. Two-Dimensional Materials: Polyphony in B Flat. *Nat. Chem.* **2016**, *8* (6), 525–527.
- (27) Lu, H.; Mu, Y.; Bai, H.; Chen, Q.; Li, S.-D. Binary Nature of Monolayer Boron Sheets from Ab Initio Global Searches. *J. Chem. Phys.* **2013**, *138* (2), 24701.
- (28) Penev, E. S.; Bhowmick, S.; Sadrzadeh, A.; Yakobson, B. I. Polymorphism of Two-Dimensional Boron. *Nano Lett.* **2012**, *12* (5), 2441–2445.
- (29) Boustani, I.; Quandt, A.; Hernández, E.; Rubio, A. New Boron Based Nanostructured Materials. *J. Chem. Phys.* **1999**, *110* (6), 3176–3185.

- (30) Boustani, I.; Zhu, Z.; Tománek, D. Search for the Largest Two-Dimensional Aggregates of Boron: An Ab Initio Study. *Phys. Rev. B* **2011**, *83* (19), 193405.
- (31) Patel, R. B.; Chou, T.; Iqbal, Z. Synthesis of Boron Nanowires, Nanotubes, and Nanosheets. *J. Nanomater.* **2015**, *2015*.
- (32) Lee, R. K. F.; Cox, B. J.; Hill, J. M. The Geometric Structure of Single-Walled Nanotubes. *Nanoscale* **2010**, *2* (6), 859.
- (33) Singh, A. K.; Sadrzadeh, A.; Yakobson, B. I. Probing Properties of Boron α -Tubes by Ab Initio Calculations. *Nano Lett.* **2008**, *8* (5), 1314–1317.
- (34) Ge, L.; Lei, S.; Hart, A. H. C.; Gao, G.; Jafry, H.; Vajtai, R.; Ajayan, P. M. Synthesis and Photocurrent of Amorphous Boron Nanowires. *Nanotechnology* **2014**, *25* (33), 335701.
- (35) Quandt, A.; Boustani, I. Boron Nanotubes. *ChemPhysChem* **2005**, *6* (10), 2001–2008.
- (36) Hnyk, D.; McKee, M. L.; Popov, I. A.; Boldyrev, A. I.; Hnyk, D.; McKee, M. L.; Popov, I. A.; Boldyrev, A. I. *Boron*; Hnyk, D., McKee, M., Eds.; Springer International Publishing: Cham, 2015.
- (37) Yakobson, B. I.; Sadrzadeh, A. The Boron Fullerenes. *Handb. Nanophysics Clust. Fullerenes* **2009**, *3*, 47.1-47.9.
- (38) Muya, J. T.; Lijnen, E.; Nguyen, M. T.; Ceulemans, A. The Boron Conundrum: Which Principles Underlie the Formation of Large Hollow Boron Cages? *ChemPhysChem* **2013**, *14* (2), 346–363.

- (39) Zhai, H.-J.; Zhao, Y.-F.; Li, W.-L.; Chen, Q.; Bai, H.; Hu, H.-S.; Piazza, Z. a; Tian, W.-J.; Lu, H.-G.; Wu, Y.-B.; et al. Observation of an All-Boron Fullerene. *Nat. Chem.* **2014**, *6* (8), 727–731.
- (40) Chacko, S.; Kanhere, D. G.; Boustani, I. Ab Initio Density Functional Investigation of B₂₄ Clusters: Rings, Tubes, Planes, and Cages. *Phys. Rev. B* **2003**, *68* (3), 35414.
- (41) Tandy, P.; Yu, M.; Leahy, C.; Jayanthi, C. S.; Wu, S. Y. Next Generation of the Self-Consistent and Environment-Dependent Hamiltonian: Applications to Various Boron Allotropes from Zero- to Three-Dimensional Structures. *J. Chem. Phys.* **2015**, *142* (12), 124106.
- (42) Yu, X.; Li, L.; Xu, X.-W.; Tang, C.-C. Prediction of Two-Dimensional Boron Sheets by Particle Swarm Optimization Algorithm. *J. Phys. Chem. C* **2012**, *116* (37), 20075–20079.
- (43) Amsler, M.; Botti, S.; Marques, M. a L.; Goedecker, S. Conducting Boron Sheets Formed by the Reconstruction of the Alpha-Boron (111) Surface. *Phys. Rev. Lett.* **2013**, *111* (13), 136101.
- (44) Cui, Z.-H.; Jimenez-Izal, E.; Alexandrova, A. N. Prediction of Two-Dimensional Phase of Boron with Anisotropic Electric Conductivity. *J. Phys. Chem. Lett.* **2017**, 1224–1228.
- (45) Feng, B.; Zhang, J.; Liu, R. Y.; Iimori, T.; Lian, C.; Li, H.; Chen, L.; Wu, K.; Meng, S.; Komori, F.; et al. Direct Evidence of Metallic Bands in a Monolayer Boron Sheet. *Phys. Rev. B - Condens. Matter Mater. Phys.* **2016**, *94* (4), 2–6.
- (46) Massote, D. V. P.; Liang, L.; Kharche, N.; Meunier, V. Electronic, Vibrational, Raman,

and Scanning Tunneling Microscopy Signatures of Two-Dimensional Boron Nanomaterials. *Phys. Rev. B - Condens. Matter Mater. Phys.* **2016**, *94* (19), 1–9.

- (47) Tsafack, T.; Yakobson, B. I. Thermomechanical Analysis of Two-Dimensional Boron Monolayers. *Phys. Rev. B - Condens. Matter Mater. Phys.* **2016**, *93* (16), 1–7.
- (48) Sun, H.; Li, Q.; Wan, X. G. First-Principles Study of Thermal Properties of Borophene. *Phys. Chem. Chem. Phys.* **2016**, *18*, 14927–14932.
- (49) Peng, B.; Zhang, H.; Shao, H.; Xu, Y.; Zhang, R.; Zhu, H. The Electronic, Optical, and Thermodynamic Properties of Borophene from First-Principles Calculations. *J. Mater. Chem. C* **2016**, *4* (16), 3592–3598.
- (50) Peng, B.; Zhang, H.; Shao, H.; Ning, Z.; Xu, Y.; Lu, H.; Zhang, D. W.; Zhu, H. Stability and Strength of Atomically Thin Borophene from First Principles Calculations. **2016**, 1–13.
- (51) Penev, E. S.; Kutana, A.; Yakobson, B. I. Can Two-Dimensional Boron Superconduct? *Nano Lett.* **2016**, *16* (4), 2522–2526.
- (52) Zhao, Y.; Zeng, S.; Ni, J. Superconductivity in Two-Dimensional Boron Allotropes. *Phys. Rev. B* **2016**, *93* (1), 14502.
- (53) Zhao, Y.; Zeng, S.; Ni, J. Phonon-Mediated Superconductivity in Borophenes. *Appl. Phys. Lett.* **2016**, *108* (24).
- (54) Cheng, C.; Sun, J.-T.; Liu, H.; Fu, H.-X.; Zhang, J.; Chen, X.-R.; Meng, S. Suppressed Superconductivity in Substrate-Supported β_{12} Borophene by Tensile Strain and Electron

Doping. *2D Mater.* **2017**, *4* (2), 25032.

- (55) Xiao, R. C.; Shao, D. F.; Lu, W. J.; Lv, H. Y.; Li, J. Y.; Sun, Y. P. Enhanced Superconductivity by Strain and Carrier-Doping in Borophene: A First Principles Prediction. *Appl. Phys. Lett.* **2016**, *109* (12), 1–6.
- (56) Gao, M.; Li, Q.-Z.; Yan, X.-W.; Wang, J. Prediction of Phonon-Mediated Superconductivity in Borophene. *Phys. Rev. B* **2017**, *95* (2), 24505.
- (57) Xiao, H.; Cao, W.; Ouyang, T.; Guo, S.; He, C.; Zhong, J. Lattice Thermal Conductivity of Borophene from First Principle Calculation. *Sci. Rep.* **2017**, No. March, 1–8.
- (58) Jiang, H. R.; Lu, Z.; Wu, M. C.; Ciucci, F.; Zhao, T. S. Borophene: A Promising Anode Material Offering High Specific Capacity and High Rate Capability for Lithium-Ion Batteries. *Nano Energy* **2016**, *23*, 97–104.
- (59) Zhang, X.; Hu, J.; Cheng, Y.; Yang, H. Y.; Yao, Y.; Yang, S. A. Borophene as an Extremely High Capacity Electrode Material for Li-Ion and Na-Ion Batteries. *Nanoscale* **2016**, *8* (33), 15340–15347.
- (60) Liang, P.; Cao, Y.; Tai, B.; Zhang, L.; Shu, H.; Li, F.; Chao, D.; Du, X. Is Borophene a Suitable Anode Material for Sodium Ion Battery? *J. Alloys Compd.* **2017**, *704*, 152–159.
- (61) Rao, D.; Zhang, L.; Meng, Z.; Zhang, X.; Wang, Y.; Qiao, G.; Shen, X.; Xia, H.; Liu, J.; Lu, R. Ultrahigh Energy Storage and Ultrafast Ion Diffusion in Borophene-Based Anodes for Rechargeable Metal Ion Batteries. *J. Mater. Chem. A Mater. energy Sustain.* **2017**, *5*, 2328–2338.

- (62) Zhang, Y.; Wu, Z. F.; Gao, P. F.; Zhang, S. L.; Wen, Y. H. Could Borophene Be Used as a Promising Anode Material for High-Performance Lithium Ion Battery? *ACS Appl. Mater. Interfaces* **2016**, *8* (34), 22175–22181.
- (63) Mortazavi, B.; Rahaman, O.; Ahzi, S.; Rabczuk, T. Flat Borophene Films as Anode Materials for Mg , Na or Li-Ion Batteries with Ultra High Capacities : A First-Principles Study. *Appl. Mater. Today* **2017**, *8*, 60–67.
- (64) Kulish, V. V. Surface Reactivity and Vacancy Defects in Single-Layer Borophene Polymorphs. *Phys. Chem. Chem. Phys.* **2017**, *19* (18), 11273–11281.
- (65) Shi, L.; Ling, C.; Ouyang, Y.; Wang, J. High Intrinsic Catalytic Activity of Two-Dimensional Boron Monolayers for Hydrogen Evolution Reaction. *Nanoscale* **2016**, *2*, 533–537.
- (66) Si, C.; Sun, Z.; Liu, F. Strain Engineering of Graphene: A Review. *Nanoscale* **2016**, *8* (6), 3207–3217.
- (67) Levy, N.; Burke, S. A.; Meaker, K. L.; Panlasigui, M.; Zettl, A.; Guinea, F.; Neto, A. H. C.; Crommie, M. F. Strain-Induced Pseudo-Magnetic Fields Greater Than 300 Tesla in Graphene Nanobubbles. *Science (80- .)* **2010**, *329* (5991), 544 LP-547.
- (68) Couto, N. J. G.; Costanzo, D.; Engels, S.; Ki, D. K.; Watanabe, K.; Taniguchi, T.; Stampfer, C.; Guinea, F.; Morpurgo, A. F. Random Strain Fluctuations as Dominant Disorder Source for High-Quality on-Substrate Graphene Devices. *Phys. Rev. X* **2014**, *4* (4), 41019.

- (69) Lu, P.; Wu, X.; Guo, W.; Zeng, X. C. Strain-Dependent Electronic and Magnetic Properties of MoS₂ Monolayer, Bilayer, Nanoribbons and Nanotubes. *Phys. Chem. Chem. Phys.* **2012**, *14* (37), 13035–13040.
- (70) Lloyd, D.; Liu, X.; Christopher, J. W.; Cantley, L.; Wadehra, A.; Kim, B. L.; Goldberg, B.; Swan, A. K.; Bunch, J. S. Band Gap Engineering with Ultralarge Biaxial Strains in Suspended Monolayer MoS₂. *Nano Lett.* **2016**, *16* (9), 5836–5841.
- (71) Zhang, Z.; Yang, Y.; Penev, E. S.; Yakobson, B. I. Elasticity, Flexibility and Ideal Strength of Borophenes. **2016**, 1–13.
- (72) Pang, Z.; Qian, X.; Wei, Y.; Yang, R. Super-Stretchable Borophene. *EPL (Europhysics Lett.)* **2016**, *116* (3), 36001.
- (73) Wang, V.; Geng, W. T. Lattice Defects and the Mechanical Anisotropy of Borophene. *J. Phys. Chem. C* **2017**, *121* (18), 10224–10232.
- (74) Mortazavi, B.; Rahaman, O.; Dianat, A.; Rabczuk, T. Mechanical Responses of Borophene Sheets: A First-Principles Study. *Phys. Chem. Chem. Phys.* **2016**, *18*, 27405–27413.
- (75) Rabczuk, M. Q. L. and B. M. and T. Mechanical Properties of Borophene Films: A Reactive Molecular Dynamics Investigation. *Nanotechnology* **2016**, *27* (44), 445709.
- (76) Zhou, Y.-P.; Jiang, J.-W. Molecular Dynamics Simulations for Mechanical Properties of Borophene: Parameterization of Valence Force Field Model and Stillinger-Weber Potential. *Sci. Rep.* **2017**, *7* (February), 45516.

- (77) Giannopoulos, G. I. Mechanical Behavior of Planar Borophenes: A Molecular Mechanics Study. *Comput. Mater. Sci.* **2017**, *129*, 304–310.
- (78) Zhang, Z.; Yang, Y.; Gao, G.; Yakobson, B. I. Two-Dimensional Boron Monolayers Mediated by Metal Substrates. *Angew. Chemie Int. Ed.* **2015**, *54* (44), 13022–13026.
- (79) Adamska, L.; Sadasivam, S.; Darancet, P.; Sharifzadeh, S. Many-Body Perturbation Theory Studies of Monolayer Boron. *In preparation* **2017**.
- (80) Wang, H.; Li, Q.; Gao, Y.; Miao, F.; Zhou, X. F.; Wan, X. G. Strain Effects on Borophene: Ideal Strength, Negative Possion's Ratio and Phonon Instability. *New J. Phys.* **2016**, *18* (7).
- (81) Feng, B.; Sugino, O.; Liu, R.-Y.; Zhang, J.; Yukawa, R.; Kawamura, M.; Iimori, T.; Kim, H.; Hasegawa, Y.; Li, H.; et al. Dirac Fermions in Borophene. *Phys. Rev. Lett.* **2017**, *118* (9), 96401.
- (82) Krukau, A. V; Vydrov, O. A.; Izmaylov, A. F.; Scuseria, G. E. Influence of the Exchange Screening Parameter on the Performance of Screened Hybrid Functionals. *J. Chem. Phys.* **2006**, *125* (22), 224106.
- (83) Paier, J.; Hirschl, R.; Marsman, M.; Kresse, G. The Perdew–Burke–Ernzerhof Exchange-Correlation Functional Applied to the G2-1 Test Set Using a Plane-Wave Basis Set. *J. Chem. Phys.* **2005**, *122* (23), 234102.
- (84) Park, C.; Giustino, F.; Cohen, M. L.; Louie, S. G. Velocity Renormalization and Carrier Lifetime in Graphene from the Electron-Phonon Interaction. *Phys. Rev. Lett.* **2007**, *99* (8),

86804.

- (85) Ivanov, I. G.; Hassan, J. U.; Iakimov, T.; Zakharov, A. A.; Yakimova, R.; Janzén, E. Layer-Number Determination in Graphene on SiC by Reflectance Mapping. *Carbon N. Y.* **2014**, *77*, 492–500.
- (86) Wentzcovitch, P. G. and S. B. and N. B. and M. C. and R. C. and C. C. and D. C. and G. L. C. and M. C. and I. D. and A. D. C. and S. de G. and S. F.; Giannozzi, P.; Baroni, S.; Bonini, N.; Calandra, M.; Car, R.; Cavazzoni, C.; Ceresoli, D.; Chiarotti, G. L.; Cococcioni, M.; et al. QUANTUM ESPRESSO: A Modular and Open-Source Software Project for Quantum Simulations of Materials. *J. Phys. Condens. Matter* **2009**, *21* (39), 395502.
- (87) Troullier, N.; Martins, J. L. Efficient Pseudopotentials for Plane-Wave Calculations. *Phys. Rev. B* **1991**, *43* (3), 1993–2006.

Supporting Information

Monolayer Mirrors Under Strain: Manipulation of Optical Anisotropy in Borophene

Lyudmyla Adamska¹ and Sahar Sharifzadeh^{1,2}

¹ Department of Electrical and Computer Engineering, Boston University, Boston, Massachusetts 02215, United States

² Department of Physics and Division of Materials Science, Boston University, Boston, Massachusetts 02215, United States

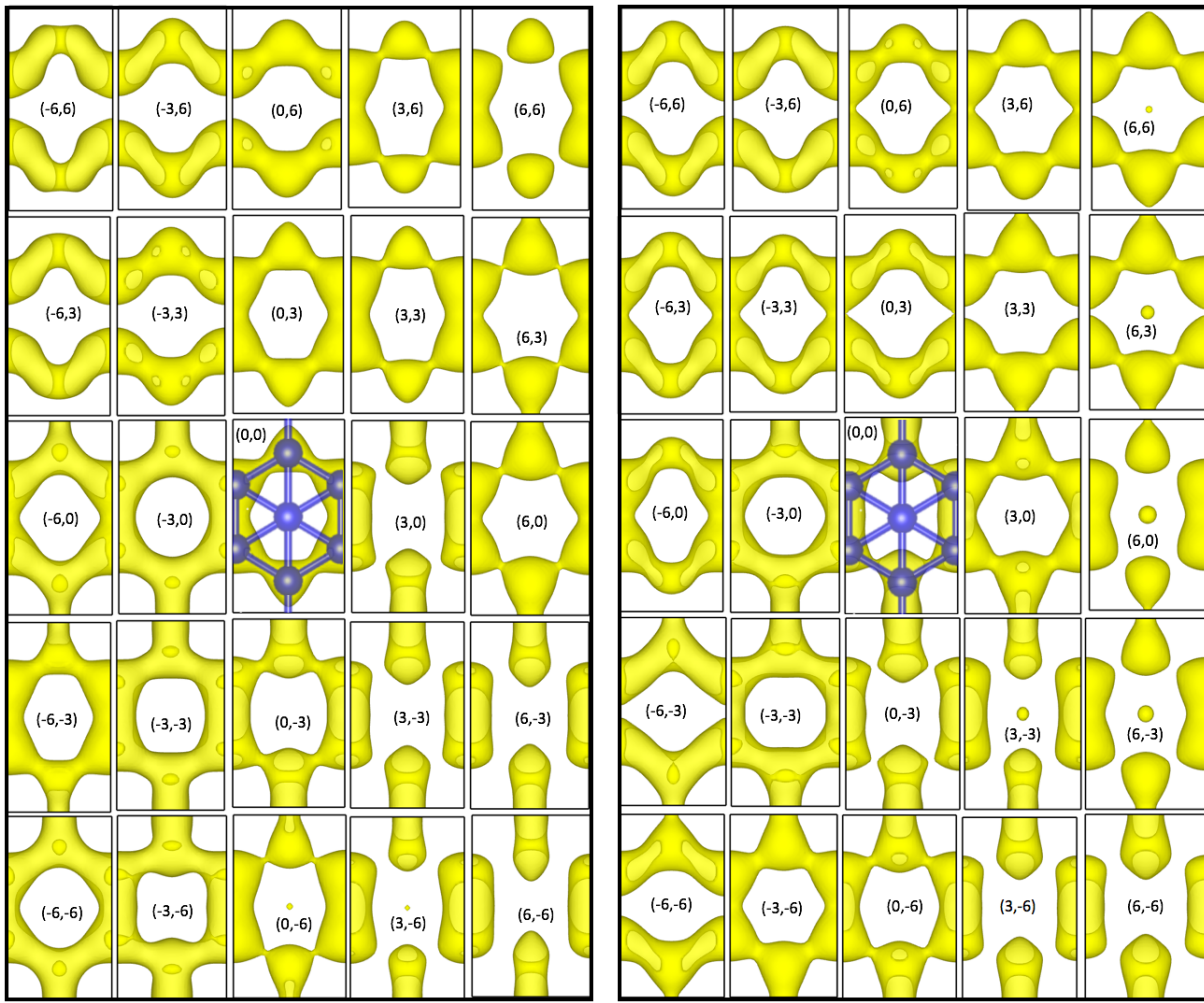


Figure S1. Local density of states (LDOS) in β_{12} borophene integrated in energy interval from the Fermi Energy (E_F) - 100 meV to E_F (left) and from E_F to $E_F + 100$ meV (right). The change in delocalization of the electronic density upon strain leads to changes in optoelectronic properties.

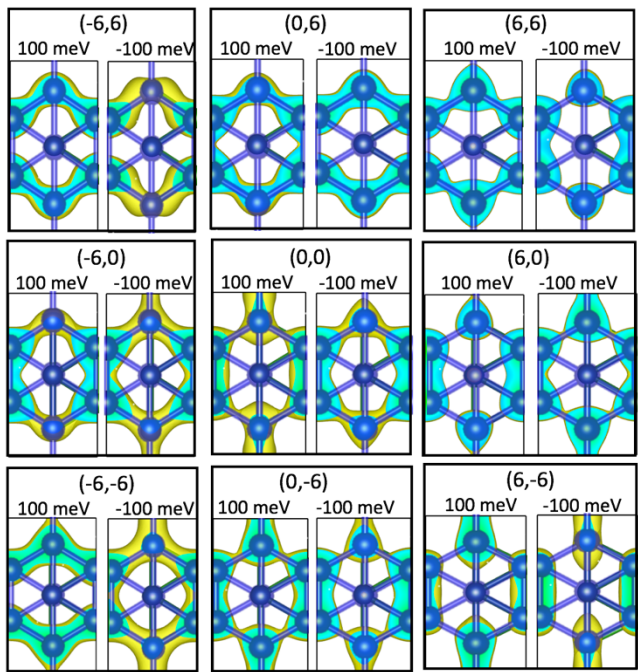


Figure S2. Slices of local density of states (LDOS) for selected values of strain in β_{12} borophene. Turquoise color corresponds to the slice of LDOS at 0.8 Å above the atomic plane.
 [What does this show that S1 doesn't?]

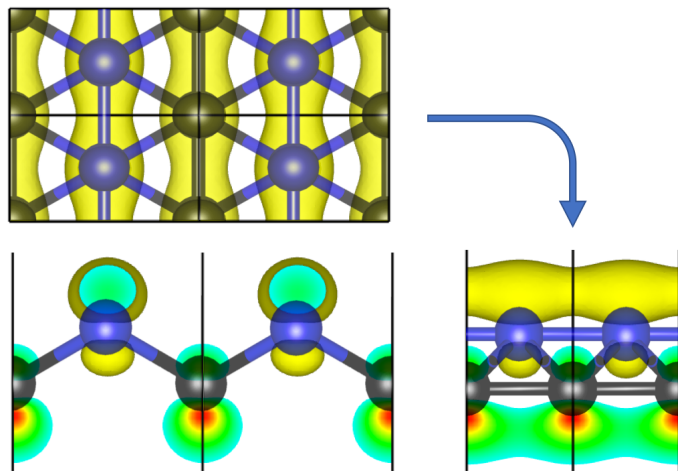


Figure S3. Isosurface of local density of states in unstrained δ_6 borophene integrated in energy interval from the Fermi energy (E_F)–100 meV to E_F . Only the unstrained structure is shown since all low and moderate strained structure show the same qualitative density distribution. The bottom panels correspond to different side projections of the top panel. The x/y- anisotropy of the charge density in this structure is apparent.

Table S1. Lattice constants of strained borophene. Negative (positive) values of strain refer to compressive (tensile) strain.

Strain, %	β_{12} structure		δ_6 structure	
	$a, \text{\AA}$	$b, \text{\AA}$	$a, \text{\AA}$	$b, \text{\AA}$
-6	2.759	4.782	2.718	1.518
-3	2.847	4.934	2.805	1.567
0	2.935	5.087	2.891	1.615
3	3.023	5.240	2.979	1.664
6	3.111	5.393	3.065	1.712

Table S2. Work function (WF) of β_{12} and δ_6 boron allotropes under applied strain. Left panel of the table shows the values of applied strain.

Strain ($\frac{a-a_0}{a_0}, \frac{b-b_0}{b_0}$) $\times 100\%$					WF of β_{12} structure, eV					WF of δ_6 structure, eV				
(-6,6)	(-3,6)	(0,6)	(3,6)	(6,6)	4.942	5.004	4.993	4.986	4.990	5.329	5.185	5.114	5.147	5.137
(-6,3)	(-3,3)	(0,3)	(3,3)	(6,3)	4.939	4.959	4.937	4.975	4.965	5.465	5.329	5.317	5.276	5.268
(-6,0)	(-3,0)	(0,0)	(3,0)	(6,0)	4.915	4.931	4.961	4.947	4.960	5.527	5.457	5.459	5.375	5.355
(-6,-3)	(-3,-3)	(0,-3)	(3,-3)	(6,-3)	4.888	4.891	4.918	4.911	4.958	5.537	5.569	5.458	5.449	5.398
(-6,-6)	(-3,-6)	(0,-6)	(3,-6)	(6,-6)	4.829	4.834	4.852	4.901	4.923	5.638	5.518	5.495	5.504	5.462

Table S3. Plasma frequencies of β_{12} borophene, which correspond to abrupt switch from high to low reflectance.

Strain ($\frac{a-a_0}{a_0}, \frac{b-b_0}{b_0}$) $\times 100\%$					$\omega_p(X)$ of β_{12} structure, eV					$\omega_p(Y)$ of β_{12} structure, eV				
(-6,6)	(-3,6)	(0,6)	(3,6)	(6,6)	3.31	3.35	3.02	2.98	2.15	0.98	1.34	1.76	1.37	1.68
(-6,3)	(-3,3)	(0,3)	(3,3)	(6,3)	3.39	3.05	3.23	2.77	2.29	1.27	1.38	1.77	2.73	2.25
(-6,0)	(-3,0)	(0,0)	(3,0)	(6,0)	3.72	3.56	3.00	2.36	2.41	0.64	2.49	1.99	1.56	2.70
(-6,-3)	(-3,-3)	(0,-3)	(3,-3)	(6,-3)	3.73	3.24	2.73	3.00	2.94	1.25	3.28	3.44	2.32	2.83
(-6,-6)	(-3,-6)	(0,-6)	(3,-6)	(6,-6)	3.02	2.75	3.91	2.59	2.38	2.92	1.32	3.15	2.30	3.01

Table S4. Plasma frequencies of δ_6 borophene, which correspond to onsets of transmittance, or abrupt switch from 100% reflectance to low reflectance.

Strain ($\frac{a-a_0}{a_0}, \frac{b-b_0}{b_0}$) $\times 100\%$					$\omega_p(X)$ of δ_6 structure, eV					$\omega_p(Y)$ of δ_6 structure, eV				
(-6,6)	(-3,6)	(0,6)	(3,6)	(6,6)	2.02	2.07	3.44	1.86	1.61	3.28	2.88	4.68	4.36	3.15
(-6,3)	(-3,3)	(0,3)	(3,3)	(6,3)	0.85	2.43	2.74	2.02	1.57	2.37	3.68	4.30	4.20	3.99
(-6,0)	(-3,0)	(0,0)	(3,0)	(6,0)	1.84	2.45	2.20	2.18	1.60	5.24	5.39	4.63	4.22	3.81
(-6,-3)	(-3,-3)	(0,-3)	(3,-3)	(6,-3)	2.33	1.93	2.06	2.03	1.43	4.20	4.92	4.14	3.86	4.45

(-6,-6)	(-3,-6)	(0,-6)	(3,-6)	(6,-6)	1.97	2.25	1.82	2.44	1.61	5.52	6.66	4.43	5.68	4.14
---------	---------	--------	--------	--------	------	------	------	------	------	------	------	------	------	------

Table S5. Approximate strength of reflectance for X- and Y- polarized light in β_{12} borophene for green light (2.5 eV energy).

Strain $(\frac{a-a_0}{a_0}, \frac{b-b_0}{b_0}) \times 100\%$					Strength of X-reflectance, %					Strength of Y-reflectance, %				
(-6,6)	(-3,6)	(0,6)	(3,6)	(6,6)	80	80	80	90	10	40	40	35	10	10
(-6,3)	(-3,3)	(0,3)	(3,3)	(6,3)	80	80	80	70	20	40	30	10	30	10
(-6,0)	(-3,0)	(0,0)	(3,0)	(6,0)	90	90	70	50	50	20	40	15	10	50
(-6,-3)	(-3,-3)	(0,-3)	(3,-3)	(6,-3)	90	70	65	70	65	20	50	60	10	55
(-6,-6)	(-3,-6)	(0,-6)	(3,-6)	(6,-6)	70	50	90	55	55	60	10	70	20	70

Table S6. Difference between plasma frequencies for X- and Y- polarized light. [Why are some values in red?]

Strain $(\frac{a-a_0}{a_0}, \frac{b-b_0}{b_0}) \times 100\%$					$\omega_p(X) - \omega_p(Y)$ of β_{12} structure, eV					$\omega_p(Y) - \omega_p(X)$ of δ_6 structure, eV				
(-6,6)	(-3,6)	(0,6)	(3,6)	(6,6)	2.3	2.0	1.3	1.6	0.5	1.3	0.6	1.2	2.5	1.5
(-6,3)	(-3,3)	(0,3)	(3,3)	(6,3)	2.1	1.7	1.5	0.0	0.0	0.5	1.3	1.6	2.2	2.5
(-6,0)	(-3,0)	(0,0)	(3,0)	(6,0)	3.1	1.1	1.0	0.8	-0.3	3.4	2.9	2.4	2.0	2.2
(-6,-3)	(-3,-3)	(0,-3)	(3,-3)	(6,-3)	2.5	0.0	-0.7	0.7	0.1	1.9	3.0	2.1	1.8	3.0
(-6,-6)	(-3,-6)	(0,-6)	(3,-6)	(6,-6)	0.1	1.4	0.8	0.3	-0.6	3.6	4.4	2.6	3.2	2.5

Table S7. Anisotropy of reflectance in borophene.

Strain $(\frac{a-a_0}{a_0}, \frac{b-b_0}{b_0}) \times 100\%$					Anisotropy of β_{12} structure, eV					Anisotropy of δ_6 structure, eV				
(-6,6)	(-3,6)	(0,6)	(3,6)	(6,6)	↑	↑	↑	↑	↓	↓	↓	↓	↑	↓
(-6,3)	(-3,3)	(0,3)	(3,3)	(6,3)	↑	↑	↑	↓	↓	↓	↓	↓	↓	↑
(-6,0)	(-3,0)	(0,0)	(3,0)	(6,0)	↑	↑	—	↓	↓	↑	↑	—	↓	↓
(-6,-3)	(-3,-3)	(0,-3)	(3,-3)	(6,-3)	↑	↓	↓	↓	↓	↓	↑	↓	↓	↑
(-6,-6)	(-3,-6)	(0,-6)	(3,-6)	(6,-6)	↓	↓	↓	↓	↓	↑	↑	↑	↑	↑